LPMO-like activity of bioinspired copper complexes: from model substrate to extended polysaccharides

Rébecca Leblay, Rafael Delgadillo-Ruiz, Christophe Decroos, Christelle Hureau, Marius Réglier, Ivan Castillo Pérez, Bruno Faure, A. Jalila Simaan

10.1002/cctc.202300933

WILEY VCH

RESEARCH ARTICLE

LPMO-like activity of bioinspired copper complexes: from model substrate to extended polysaccharides

Rébecca Leblay,[a] Rafael Delgadillo-Ruíz,[b] Christophe Decroos,[a,d] Christelle Hureau,[c] Marius Réglier,[a] Ivan Castillo,[b]* Bruno Faure [a] and A. Jalila Simaan[a]*

[a] R. Leblay, Dr. C. Decroos, Dr. Marius Réglier Dr. B. Faure, Dr. A. J. Simaan
Aix Marseille Univ, CNRS, Centrale Marseille, iSm2, Marseille, France
E-mail: jalila.simaan@univ-amu.fr
[b] R. Delgadillo-Ruíz, Dr. I. Castillo
Instituto de Química, UNAM
Circuito Exterior, Ciudad Universitaria
México, 04510 (México)
E-mail : joseivan@unam.mx
[c] Dr. Christelle Hureau
Laboratoire de Chimie de Coordination, CNRS, UPR 8241
205 route de Narbonne,
31077 Toulouse (France)
[d] present address for Dr. C Decroos
Université de Strasbourg, CNRS, INSERM
IGBMC, UMR 7104,
67404 Illkirch, France

Supporting information for this article is given via a link at the end of the document.

Abstract: Polysaccharide oxidative depolymerization is highly desirable to achieve recalcitrant biomass valorization. Inspired by recently discovered Lytic Polysaccharide Monooxygenases, mononuclear copper complexes have been prepared and studied in the literature. However, the activities were evaluated on different substrates and under various conditions. In this work we intended to establish a robust and reproducible activity assay, in aqueous solution at a pH close from neutrality and under mild conditions. We have evaluated several complexes on substrates of increasing complexity: the model substrate para-nitrophenyl-β-D-glucopyranoside (*p*-NPG), cellobiose (glucose dimer), as well as on extended substrates (chitin, cellulose and bagasse from agave). The different assays were compared and proof-of-concept that bioinspired complexes can oxidatively promote polysaccharide depolymerization was obtained. Finally, we measured level of hydroxyl radicals released by the complexes under comparable experimental conditions and mechanistic pathways are discussed.

Introduction

Lignocellulosic biomass is increasingly considered as a renewable feedstock to produce bio-sourced chemicals, biomaterials and advanced biofuels.[1] It is composed of three main biopolymers: cellulose, hemicellulose, and lignin that are intricated in a solid and recalcitrant assembly.[2,3] One important step in the valorization of biomass components into valuable products consists in size reduction of the polymers. In this context, Lytic Polysaccharide Monooxygenases (LPMO), discovered in 2010, have attracted attention given their ability to initiate the degradation of recalcitrant polysaccharides from biomass.[4–7] LPMO are mono-copper enzymes able to promote extended polysaccharides cleavage (*e.g.* cellulose or chitin) using oxidative mechanisms.[4,8,9] More precisely, LPMO catalyze the hydroxylation of an inert C-H bond at the glycosidic linkage (either at C1 or C4 position) at the surface of recalcitrant polysaccharide polymers further leading to glycosidic bond cleavage (Fig 1A). This leads to a decrease of polysaccharide crystallinity, rendering them more amenable to further degradation by traditional hydrolytic enzymes.[10,11] Several subfamilies of LPMO from various organisms (mainly fungi and bacteria) have been characterized and classified.[12] They display a very conserved surface-exposed metal coordination motif, named “histidine brace”,[13,14] composed of two histidines including the *N*-terminal histidine that is coordinated to the copper ion in a bidentate fashion (Fig 1B).

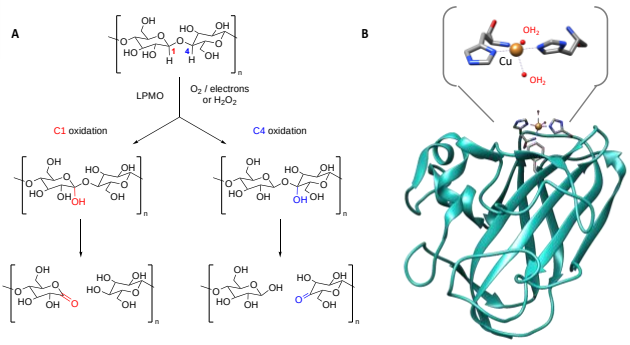

Figure 1. (**A**) C1 or C4 hydroxylation of cellulose catalysed by LPMO, leading to chain cleavage (**B**) structure of a bacterial LPMO[15] with its surface-exposed active site and view of the conserved copper coordinating ligands.

To perform hydroxylation of the strong C-H bonds at the glycosidic linkage, LPMO requires an oxygenated co-substrate. The exact nature of this oxygenated co-substrate (dioxygen or hydrogen peroxide) is still debated.[3,16–19] Interestingly, LPMOs could turn out to be H_2O_2-dependent peroxygenases instead of O_2-dependent oxygenases.[8] In all cases, it has been proposed that the resting copper(II) enzyme is reduced to the copper(I) state prior to reaction with either of the co-substrates (Scheme 1). Both pathways would produce a common Cu(I)-(H_2O_2) intermediate

10.1002/cctc.202300933

followed by the generation of hydroxyl radicals in a controlled Fenton-type reactivity.[16,17,20] In the case of Fe-dependent peroxidases, a similar Fenton-type pathway has been discussed and HO• radicals, stabilized and positioned within the active site, are likely responsible for selective oxidation of the substrate. In the case of LPMO, HO• radicals would rather perform H-abstraction from Cu(II)−OH, generating a highly reactive Cu(II)-O• species that would be the actual hydrogen-abstracting intermediate.[21]

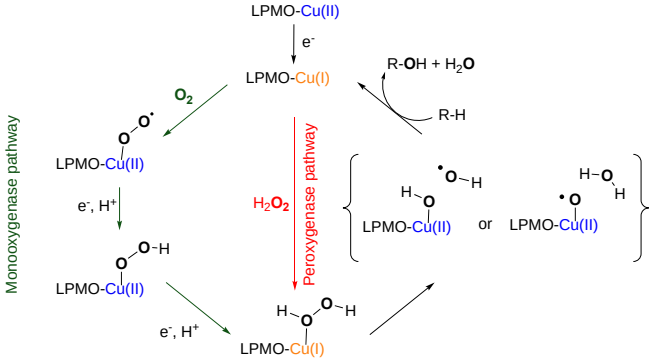

Scheme 1. proposed mechanistic pathways for LPMO activity using either O_2 (monooxygenase) or H_2O_2 (peroxygenase) as co-substrate.

The development of bioinspired model complexes has allowed getting substantial mechanistic information on dioxygen activation pathways in copper-containing systems.[22–27] It can also be a strategy to develop bioinspired catalysts. The growing interest in recalcitrant polysaccharides valorization as well as in LPMO mechanistic studies has fueled the development of structural and functional copper-containing mimics of LPMO. A few years ago, Concia *et al*. have reported two complexes with N_3-coordination motifs ([(**PyA**)Cu(CH_3CN)](ClO_4)$_2$ and [(**PyI**)Cu(OH_2)](ClO_4)$_2$ using **PyA** and **PyI** ligands, Scheme 2) and tested them for the oxidative cleavage of a model substrate, para-nitrophenyl-β-D-glucopyranoside (*p*-NPG), in presence of hydrogen peroxide in aqueous solutions.[28] The initial product formation rates were found up to 6 times higher than that of a copper salt under the same conditions and after 24h, up to 50 TON were achieved. An intermediate was detected and attributed to a mononuclear Cu(II)-OOH species. In the meanwhile, Neira *et al*. have studied a bis-benzimidazole based complex, [(**2BB**)Cu(OH_2)$_2$](OTf)$_2$ (Scheme 1) as a structural and functional mimic of LPMO.[29,30] Its oxidative activity was evaluated on cellobiose and glucose in aqueous solutions under various conditions. Both **2BB**-based Cu(I) and Cu(II) complexes were competent sources for oxidative cellobiose degradation, with H_2O_2 as better oxidant than O_2 or KO_2. The key intermediate detected was assigned to a bridging peroxo dicopper(II) species.[30]

Since these first reports, several complexes modelling the coordination sphere of LPMO were prepared using conventional *N*-based ligands (pyridines, (benz)imidazoles, amines).[31–37] or aminoacid/peptide-based ligands to reproduce the primary amine ligation found in the enzymatic system.[38–40] A variety of substrates were used to evaluate their activity ranging from simple benzyl alcohol[38] to soluble substrates (*p*-NPG,[31,32,37,39] cellobiose,[35] *p*-NP-glycosidic substrates[33]) and one report on the use of insoluble cellulosic substrate.[34]

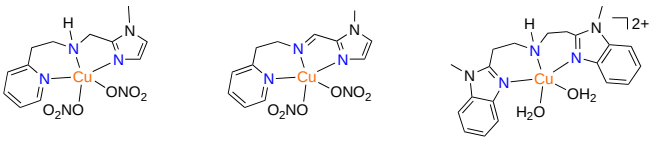

Scheme 2. Complexes used in this study.

The variety of substrates and reaction conditions used to evaluate LPMO-like activity of the mimics renders comparison and structure-activity relationships complicated. We were therefore interested in establishing a simple and reproducible LPMO-like activity assay for bioinspired model complexes. Herein, we selected three complexes, **PyA-Cu**, **PyI-Cu**, **2BB-Cu** (Scheme 2), to carry out systematic assays on different substrates of increasing complexity to compare the robustness of the assays and the performance of the catalysts. The assays were performed in buffered solutions at pH 7.5 and using hydrogen peroxide as co-substrate (in a peroxide-shunt approach). The complexes were first tested using the model substrate *p*-NPG, then on cellobiose, a real glycosidic substrate. Finally, we evaluated the mimics activity on two polymeric substrates (chitin and cellulose) and on a complex substrate (bagasse from agave). To gain insight into the nature of oxidizing species (metal-centered *vs*. hydroxyl radicals) we evaluated the amount of hydroxyl radicals released by the complexes under similar reaction conditions.

Results and Discussion

Preparation and characterization of complexes

The complexes were prepared following previously reported procedures.[28,29] In order to avoid the use of potentially explosive perchlorate salts, **PyA-Cu** and **PyI-Cu** were prepared using nitrate counter anions. Crystals suitable for X-ray crystallographic analysis were obtained and the newly solved structures are displayed in Figure 2 (additional data in Table S1 and S2). These structures are highly similar to those reported with perchlorate counter ions.[28]

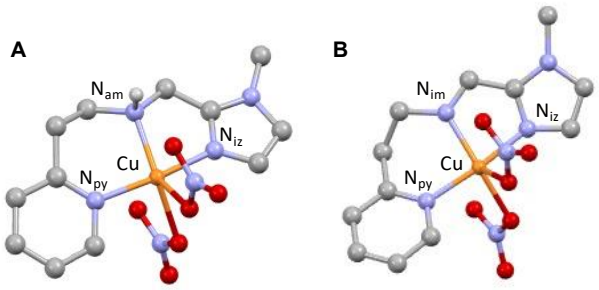

Figure 2. Representation of the crystallographic structures of [(**PyA**)Cu^{II}(NO_3)$_2$] (A) and [(**PyI**)Cu^{II}(NO_3)$_2$] (B). Hydrogen atoms were omitted for clarity (except the one on the secondary amine of **PyA**).

10.1002/cctc.202300933

In both cases, the copper(II) ions are found in distorted square-pyramidal geometry with the nitrogen donors from the ligands (**PyA** and **PyI** respectively) and one oxygen atom from the nitrate counter ions in the basal plane. The second nitrate is coordinated in apical position. Cu-N distances range from 1.98 Å to 2.05 Å (Table S2). These distances are comparable to those obtained for the same complexes with perchlorate counter anions and are also in good agreement with the distances found in the biological active site.[14]

In order to characterize the complexes in solution, Electron Paramagnetic Resonance (EPR) measurements were carried out in frozen solutions. EPR spectra or [(**PyA**)$Cu^{II}(NO_3)_2$] and [(**PyI**)$Cu^{II}(NO_3)_2$] were measured in phosphate buffer set at pH 7.5 (Figure S1) and EPR parameters derived from simulation are displayed in Table 1. The EPR parameters are highly similar to those obtained in the case of perchlorate counter ions and are consistent with Cu(II) ions in square-pyramidal geometries with [3N,1O] donors coordinated in the basal plane.[41,42] The structures of the complexes are therefore mainly retained in solution. It is probable that the counter ions de-coordinate and are exchanged by water molecules as previously observed in the case of the perchlorate complexes and as supported by ESI-MS data (see experimental section). The EPR spectrum of 0.2 mM solution of [(**2BB**)$Cu(OH_2)_2$]$(OTf)_2$ in phosphate buffer indicates the presence of mononuclear copper centers in distorted trigonal bipyramidal geometry (Figure S2). The EPR parameters (Table 1) of these mononuclear entities are coherent with the solid-state structure and previously reported EPR data.[29]

Table 1. EPR parameters and redox properties of the complexes placed in phosphate buffer at pH 7.5. EPR spectra were recorded at 120K using 0.2 mM concentration in the presence of 10% glycerol.

LCu^{II}	Relevant EPR parameter (A in MHz)						Redox prop. (mV *vs*. SHE)
	g_z	g_y	g_x	A_z	A_y	A_x	$E_{1/2}$
PyI	2.265	2.072	2.049	535	<50	<50	50
PyA	2.260	2.067	2.049	530	<50	<50	-25
2BB	2.242	2.120	2.010	320	180	270	265

We then determined the redox potentials of the complexes by cyclic voltammetry (Fig. S3 and Table S3). The CV curves reveal quasi-reversible Cu(II)/Cu(I) redox processes with $E_{1/2}$ of -25 and 50 mV *vs*. SHE for **PyA** and **PyI**-based complexes respectively (Table 2). In the case of **2BB-Cu** complex, the redox potential is higher at $E_{1/2}$ = 265 mV *vs*. SHE. These data are comparable to those already reported.[28,30] Notably, **2BB-Cu** displays a redox potential similar to that of LPMO enzymes that were determined to range within 200-330 mV *vs*. SHE.[18,43–48]

LPMO-like activity on para-nitrophenyl β-(D)-glucopyranoside (*p*-NPG)

LPMO-like activities of bioinspired copper complexes were first evaluated on the "model substrate", para-nitrophenyl-β-(D)-glucopyranoside (*p*-NPG). The formation of the chromophore, *p*-nitrophenolate (*p*-NPO^-) is followed spectrophotometrically at 400 nm and initial rates are extracted (Fig. S4). It has to be noted that the pKa of the phenol moiety is *ca*. 7.1. The intense absorption at 400 nm is linked to the basic form of the chromophore and at the chosen pH for the catalytic assays, part of the phenol remains protonated (*ca*. 25-30%). As displayed in Figure 3, *p*-NPO(H) formation rate increases with the concentration of catalysts and tends to a plateau at higher concentrations. It reveals that, at all concentrations, **PyI-Cu** and **PyA-Cu** produce *p*-NPO(H) with higher initial velocities than copper nitrate in the same conditions (up to two times higher). On the contrary, *p*-NPO(H) production in the presence of **2BB-Cu** is slower than in the presence of other catalysts at all concentrations. The dependance of the initial rate with catalysts concentration is not linear indicating that simple Michaelis-Menten model does not apply here and that the rate law is probably more complex (Fig. S5).

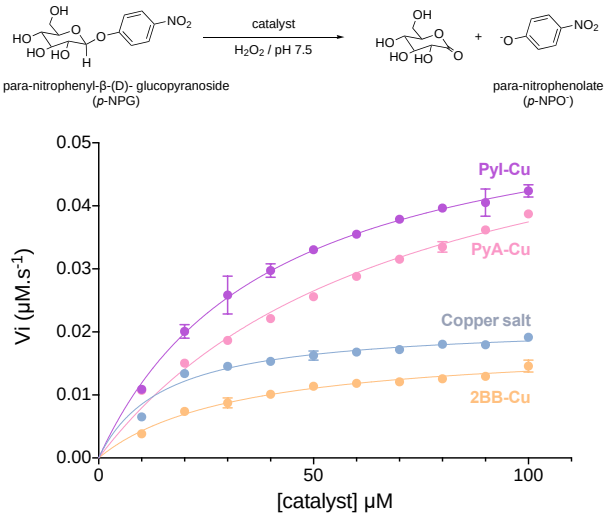

Figure 3. Initial velocity of formation of *p*-NPO(H) as a function of the concentration of catalyst. Conditions: 10 mM phosphate buffer pH 7.5; [*p*-NPG] = 10 mM and [H_2O_2] = 40 mM, temperature = 30°C. The lines do not represent fits but data interpolation.

The same trend is observed on the product's formation after 20 minutes and **PyI-Cu** complex appears to produce up to 1.5 times more *p*-NPO(H) than free copper (Fig. 4A). We have verified that in absence of hydrogen peroxide and/or catalyst, no significant amount of product is formed, consistent with the involvement of oxidative pathways. In order to verify the reliability of this assay, we explored the ability of the complexes to oxidize the produced *p*-NPOH/*p*-NPO^-. Experiments were thus conducted using the chromophore as substrate and monitoring the decrease of absorbance at 400 nm under different experimental conditions (Fig. 4B). When using 20 µM of *p*-NPO(H) in the assay, a quantity that is representative of the amount formed upon cleavage of *p*-NPG after 20 minutes, a significant *p*-NPO(H) consumption is observed (up to 10 µM of chromophore are consumed within 20 minutes). These results suggest that the catalysts can further oxidize/degrade *p*-NPO(H) into compounds that do not absorb at 400 nm. This subsequent reactivity can induce significant bias when comparing the activity of the catalysts and probably leads to underestimation of the activity. It has to be noted that no significant consumption of chromophore is detected in control experiments (complexes alone without H_2O_2 or in the absence of catalyst). Noteworthy, the best catalyst for *p*-NPG degradation (**PyI-Cu**) is also leading to important consumption of the *p*-NPO(H) chromophore. This spectrophotometric assay has been

10.1002/cctc.202300933

widely used in the literature to estimate the LPMO-like activity of copper complexes.[28,31,32,37,39] These control experiments imply that a lot of care must be taken when performing and interpreting this simple and convenient spectrophotometric assay.

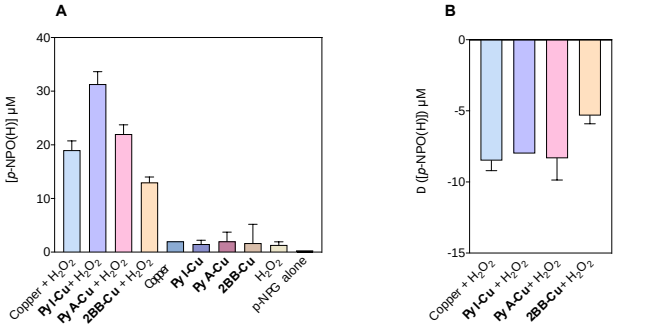

Figure 4. (A) Conversion of para-nitrophenyl-β-(D)-glucopyranoside (*p*-NPG) in para-nitrophenol(ate) (*p*-NPO(H)) after 20 minutes, with [catalyst] = 10 µM, [H_2O_2] = 40 mM and [*p*-NPG] = 10 mM (B) decay of concentration of *p*-NPO(H) after 20 minutes, with [catalyst] = 10 µM, [H_2O_2] = 40 mM and [*p*-NPO(H)] = 20 µM, temperature = 30°C.

LPMO-like activity on cellobiose

The catalysts were evaluated on a soluble oligosaccharide, cellobiose (G2), a dimer of glucose linked by a β-1,4 glycosidic bond. This substrate has the advantage of being soluble while displaying a real glycosidic bond. Given the similar behavior of **Pyl-Cu** and **PyA-Cu** on *p*-NPG, we compared **Pyl-Cu** and **2BB-Cu** to free copper for the oxidation of cellobiose.

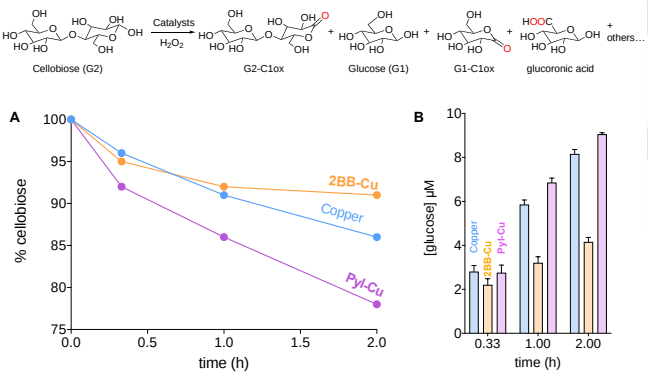

Figure 5. Oxidation of cellobiose and products identified on the chromatogram. (A) Decay of cellobiose (% of remaining G2) as a function of time (B) Concentration of glucose (G1) released during the same experiment. [cellobiose] = 200 µM, [H_2O_2] = 2 mM and [catalyst] = 20 µM in 10 mM phosphate buffer pH=7.5 (30°C).

Cellobiose was incubated with the catalysts and hydrogen peroxide and the products were analyzed using HPAEC-PAD. Different products could be identified after reaction (Fig. 5 and Fig. S6): glucose (G1), gluconic acid (G1-C1ox), cellobionic acid (G2-C1ox) and glucuronic acid (C6 oxidation). The low response factor for some compounds (Fig. S7), associated with the presence of several unidentified and overlapping products (possibly including doubly oxidized products) complicated the quantification. Therefore, the reactivity was evaluated by quantifying the decrease in substrate's (G2) concentration (Fig 5A). After two hours of reaction with **Pyl-Cu**, cellobiose concentration dropped to reach 78% of its initial concentration, *i.e*. slightly more than 40 µM of G2 were consumed (2 TON). When increasing H_2O_2 concentration, the quantity of cellobiose drops to 45% of the initial one (Fig. S8) which corresponds to *ca*. 105 µM of G2 transformed in one hour (5 TON). In the case of copper and of **2BB-Cu**, G2 concentrations were measured to 86 % and 91 % of the initial concentrations respectively (Fig. 5). **2BB-Cu** activity reaches a plateau after *ca*. 30 minutes in contrast to free copper and **Pyl-Cu**. This possibly indicates a modification of the complex leading to loss of activity. This is not compatible with a degradation of the complex that would release copper in solution since free copper displays higher activity towards cellobiose. After 24 hours, **Pyl-Cu** is able to consume almost 70% of the cellobiose (*i.e*. 140 µM of G2 consumed, Fig. S9). This value is however very similar to that obtained with copper nitrate, suggesting that **Pyl-Cu** undergoes damages after long incubation time and that free copper may be released in solution.

In the case of C1 or C4 oxidations of G2, glucose is expected to be released in addition to C1 or C4 oxidized moieties (Fig. 1A). In the case of **Pyl-Cu**, one could expect *ca*. 40 µM of glucose produced after 2 hours. However, only 8-10 µM of glucose are detected, a quantity significantly lower than expected (Fig. 5B). This can be partly due to over-oxidation of glucose as experimentally evidenced (Fig. S10). Interestingly, although 10% of G2 has been converted after 2 hours in the presence of copper (*i.e*. 20 µM), G1 concentration is around 8 µM coherent with the fact that less over-oxidation of glucose occurs when using copper instead of **Pyl-Cu**. Finally, the amount of G1 produced when **2BB-Cu** is used as a catalyst increases slowly, consistent with a rapid loss of activity of this complex under these experimental conditions.

LPMO-like activity on insoluble substrates

Given the ability of the copper-based complexes to promote glycosidic bond cleavage of a soluble disaccharide, the activities were evaluated on more complex and insoluble substrates: chitin, cellulose, and bagasse from agave. Chitin is an abundant polysaccharide which is mainly found in the exoskeleton of insects and crustaceans. It consists in a *N*-acetylglucosamine derivative of cellulose. Agave bagasse is the main solid waste generated by the tequila industry in Mexico. It is mainly composed of polysaccharides (50-60%) but also contains lignin as it can be seen from the dark brown color of the fibers (Fig. 6).[49]

In this assay, the solid substrates were incubated during 24 hours at 30°C in the presence of the complexes and hydrogen peroxide. After incubation, the mixtures were centrifugated and the remaining solid parts were dried to evaluate the mass loss (Fig. 6). When chitin is used as substrate, up to 30% of mass loss is obtained in the presence of the catalysts. The same is observed when copper alone is used as well. This activity is metal-dependent since the weight loss in the presence of hydrogen peroxide alone is *ca*. 5%. We have investigated the effect of time and hydrogen peroxide concentration and the same tendencies are observed in all tested conditions (Fig. S11).

The difference between the complexes is more obvious when cellulose is used as substrate. Notably, **Pyl** and **PyA**-based

systems display slightly better reactivity than free copper (10-12% of weight loss *vs*. 8% respectively). However, the differences are rather modest and this probably underlines that inactivation of the complexes and copper release has occurred after long reaction times. **2BB-Cu** displays lower reactivity on cellulose under those conditions, in line with the results on soluble substrates. The soluble fractions were analyzed using HPAEC-PAD (Fig. S12). In all cases, the chromatograms reveal the presence of a mixture of products. Soluble oligosaccharides (G1, G2, and possibly G3) can be detected (200-300 μM of glucose are measured). The presence of gluconic acid (G1-C1ox) is also evidenced and confirmed by HPLC with ELSD (Evaporative Light Scattering) detection. The complexity of the mixtures (presence of unidentified and overlapping products) renders further analysis and quantification difficult.

Finally, when bagasse is used, a loss of *ca*. 18-20% is obtained with all the metal complexes and with the copper salt. However, in absence of catalyst, when hydrogen peroxide alone is used, the sample loses *ca*. 15 % of its initial mass. This is probably partly related to oxidative damage on the lignin component since the color of the sample becomes clearer after treatment.

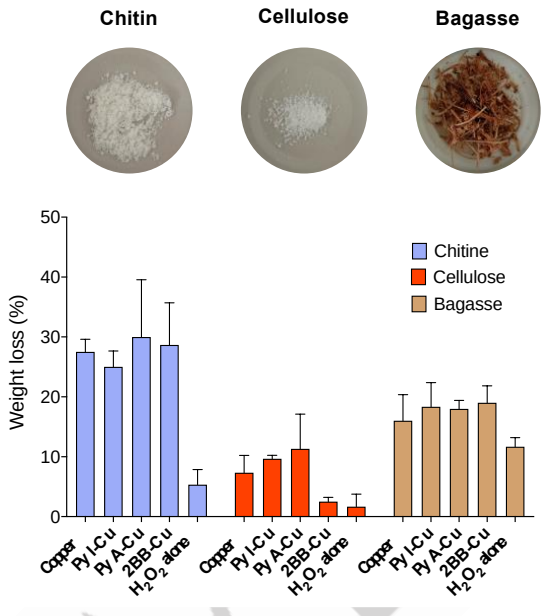

Figure 6. Loss of weight (%) for chitin, cellulose or bagasse incubated 24 hours at 30°C in the presence of catalysts (60 μM) and hydrogen peroxide (1 M) in phosphate buffer set at pH 7.5.

Mechanistic considerations

In the case of LPMO, after reaction with either dioxygen and electrons or hydrogen peroxide, it has been proposed that a controlled Fenton-type reactivity occurs (Scheme 1).[16,50] Within this mechanistic scheme, the nature of the species responsible for the strong C-H bond abstraction step could be hydroxyl radicals and/or copper-oxyl species. Similarly, the reactivity of the Cu(II) complexes in the presence of H_2O_2 may be related to a ‘‘free radical’’ *vs*. a ‘‘metal-centered” pathway.
The reaction of metal ions with hydrogen peroxide and reactive species (Reactive Oxygen Species or ROS) derived from Fenton-like reactions have been extensively studied.[51,52] Two types of ROS can be considered in our conditions: superoxide anion and hydroxyl radicals.

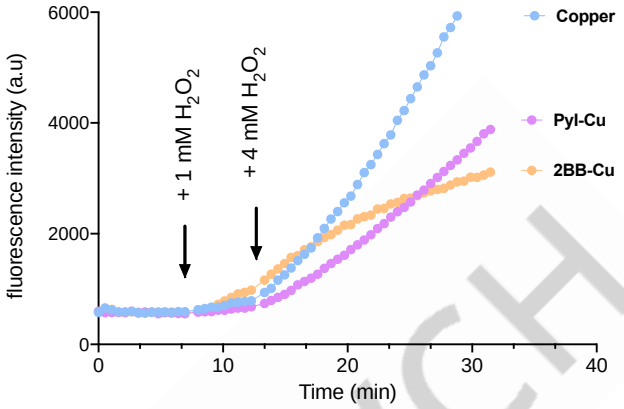

Figure 7. Evolution of the fluorescence intensity of 7-hydroxycoumarin at 452 nm (excitation at 395 nm) with time for the different complexes after addition of hydrogen peroxide. Conditions: [catalyst] = 10 μM, [CCA] = 0.5 mM, [H_2O_2] = 1 mM and then 5 mM

Superoxide anion reactivity is rather well documented and it was shown to be involved in reactions such as proton exchange, disproportionation, nucleophilic substitution, one-electron transfers etc.[53] In addition, superoxide is rather instable in aqueous solutions (due to spontaneous dismutation) and is the precursor of other ROS. We were therefore interested in quantifying the production of hydroxyl radicals in our experimental conditions. We used coumarin-3-carboxylic acid (CCA), a hydroxyl radical trap, to monitor hydroxyl radical released by the Cu complexes using a previously reported procedure.[54,55] Upon reaction with hydroxyl radicals, CCA is converted into 7-hydroxy-CCA which displays fluorescence at 450 nm when excited at 390 nm. The stepwise additions of hydrogen peroxide under the catalytic conditions (catalyst at 10 μM in 10 mM phosphate buffer at pH 7.5) leads to an increase of the fluorescence, witnessing the production of hydroxyl radicals (Fig. 7 and Fig. S13). In the case of **2BB-Cu**, the fluorescence increases rapidly, event when only 1 mM of H_2O_2 is added, and then reaches a plateau, indicating that the complex has undergone modifications and subsequently releases less radicals. This is consistent with the results from previous activity assays that suggested a rapid inactivation of this catalyst without release of free copper. When using **PyA-Cu,** the level of hydroxyl radical captured by CCA increases slower than when copper salt is used (Fig. S13). Finally, **Pyl-Cu** induces the slowest increase in hydroxyl radical concentration. Yet, reactivity data on soluble substrates (*p*-NPG and cellobiose) have indicated that **Pyl-Cu** reacts faster with the glycosidic-related substrates than copper (Fig. 5 and Fig. S8). This may indicate that different species are involved in the reactivity with the saccharide-type substrates as compared to CCA, or that **Pyl-Cu** and **PyA-Cu** grasp a part of the produced radicals, preventing them to reach CCA.

In the case of **2BB-Cu**, the formation of a dicopper side-on peroxide ($[(\mathbf{2BB})_2Cu_2(\mu\text{-}\eta^2\text{-}\eta^2\text{-}O_2)]^{2+}$) species upon reaction of **2BB-Cu** with hydrogen peroxide has been previously observed.[30] These entities are possibly formed under our

experimental conditions. In the case of **PyI-Cu** and **PyA-Cu**, mononuclear Cu(II)-OOH species were detected when the Cu(II) precursors are placed in the presence of hydrogen peroxide.[28] Mononuclear Cu(II)-OOH intermediates are generally sluggish oxidants and are rather precursors for more oxidizing species, such as Cu(II)-O$^{\bullet}$ and/or HO$^{\bullet}$ that can be formed upon O-O bond cleavage.[22–27] The binuclear *vs*. mononuclear pathways could partially account for the difference in reactivity between the systems, in line with the observation that mononuclear Cu/O intermediates are more efficient for strong C-H bond oxidation than binuclear ones.[56] In addition, the determined Cu(II)/Cu(I) redox potentials (Table 1), suggests that **2BB-Cu(I)** redox state is more stable than with the other systems. When using **2BB** ligand, Cu(I) species could more easily be generated during the course of the reaction, for example following *(i)* reduction by hydrogen peroxide (as already reported for other Cu(II) systems)[57] *(ii)* oxidative events or *(iii)* release of dioxygen from binuclear peroxo entities. The subsequent reaction of Cu(I) with hydrogen peroxide could produce hydroxyl radicals in a peroxygenase-like pathway.

In all cases, hydroxyl radicals are formed. These hydroxyl radicals are prone to induce oxidative modifications of ligands, as recently reported.[58] Consequently, understanding the inactivation pathways and optimizing the stability of the catalysts would be interesting prospects for future investigations. Notably, it has been shown that LPMO undergoes auto-oxidative and inactivation events, possibly releasing free copper as well.[8,59–61]

Conclusion

In this paper, we have evaluated three different assays for LPMO-like activity measurements of the model complexes. The first is based on a simple substrate, *p*-NPG. This substrate has the advantage of allowing spectrophotometric detection using multi-well plates, giving easy access to kinetic data. Yet, the demonstration that the best catalysts can also oxidize the *p*-NPO(H) product renders data interpretation more difficult. Care must thus be taken when using this simple and convenient assay. From our own experience, we would recommend to discuss mainly initial rates and to verify the reactivity of the complexes on the phenolic chromophore. Finally, we have previously reported on the formation of intermediate species displaying absorption at 350-400 nm (formation more pronounced at higher pH)[28] that can interfere with product's detection. Controls in absence of substrate should therefore be performed.

The second substrate, cellobiose, has the advantage of being soluble and of containing a real glycosidic bond. Substrate and products can be detected by HPAEC set up, although the detection is longer than UV-VIS spectrophotometry on multi-well plates. One advantage of this assay is the detection of oxidized products. However, the complexity of the reaction mixture is high and some products cannot be easily identified. Nonetheless, activity obtained on the two soluble substrates provide similar tendencies (Table S4), meaning that both substrates can be used for screening purposes.

Lastly, we have shown that the complexes display activity on extended substrates such as cellulose or chitin (Fig. 6). The assays are performed by quantifying the loss of mass of the solid substrates after incubation with the catalysts, a simple way to evaluate cleavage events and release of soluble fragments. These assays are easy to handle, although less sensitive than assays on soluble substrates. It has to be noted that chitin is prone to deacetylation events that can contribute to the loss of weight and that cellulose is probably a more relevant substrate in the context of glycosidic oxidative cleavage by bioinspired model complexes, which are often less selective than biological systems. Interestingly, although the complexes may have undergone inactivation processes, the nature of the ligand has a small influence on the extent of cellulose cleavage. These results on cellulose are therefore proof-of-concepts that bioinspired catalysts can promote recalcitrant polysaccharide oxidative events.

From our preliminary mechanistic investigations, it appears that, in all cases hydroxyl radicals are produced, although the complexes may display different reactivity. In the presence of **2BB-Cu**, a fast conversion of CCA into the fluorescent 7-hydroxy-CCA is observed followed by a slower phase that suggests that the complex undergoes modifications. This behavior is in line with the reactivity kinetics on *p*-NPG and cellobiose. **PyI-Cu** and **PyA-Cu** display slower reactivity on CCA than free copper although usually more reactive on saccharide-type substrates. This apparent discrepancy could be explained by the oxidation of the ligands themselves (grasping the HO° produced by the corresponding complexes) and/or by different mechanistic paths. Overall, it is probable that different mechanistic pathways are at play when different systems are used, depending on the nuclearity and/or on the redox properties of the complexes. Further work is in progress to better understand the mechanisms and to optimize the catalyst's stability.

Experimental Section

Chemicals were obtained from commercial sources and used without further purification. Microcrystalline cellulose from cotton (9004-34-6, 20µm) and chitin from shrimp shells (1398-61-4) were purchased from Sigma Aldrich. Bagasse was provided by Casa León Rojo from Eduardo Neri municipality, Guerrero state, Mexico. Elemental analysis was performed using a Thermo Finnigan EA 1112 instrument. The results were validated by at least two measurements. FT-IR spectra were recorded in attenuated total reflection (ATR) mode on a Bruker TENSOR 27 spectrometer equipped with a single-reflection DuraSamplIR diamond ATR accessory. NMR spectra were recorded on a Brucker-Avance III nanobay spectrometer (300 or 400 MHz) using TMS as internal reference. ESI-MS analyses were performed using a SYNAPT G2 HDMS (Waters) spectrometer equipped with a pneumatically assisted Atmospheric Pressure Ionization (API) source. The ion-spray voltage was 2.8 kV, the orifice lens was 20 V, and the nitrogen flux (nebulization) was 100 L h^{-1}. The HR mass spectra were obtained with a time-of-flight (TOF) analyser. The ligands **PyI**, **PyA**, **2BB** as well as the complex [(**2BB**)Cu(OH$_2$)$_2$](OTf)$_2$ (**2BB-Cu**) were synthesized according to already reported procedures.[28,29]

Synthesis of complex [(PyI)Cu(NO$_3$)$_2$]·(PyI-Cu). The ligand (0.500 g, 2.33 mmol) was dissolved in 10 ml of methanol and a water solution (5 ml) of copper(II) nitrate trihydrated (0.95 eq) was added slowly under stirring. The resulting deep blue solution was stirred for 1 hour. Then, the solution was let stand at room temperature until crystals suitable for crystallographic analysis were formed (yield = 67 %). Elemental analysis (%): N 19.67; C 33.51; H 3.74; Calcd for $C_{12}H_{14}CuN_6O_6\cdot(H_2O)_{1.5}$. N 19.60;

C 33.61; H 4.0. ESI-MS (MeOH/H_2O): m/z = 277 $[(L\text{-}H)Cu]^+$; *m/z* = 138.5 $[LCu]^{2+}$ and *m/z* = 147.5 $[LCu\text{-}(OH_2)]^{2+}$. FTIR-ATR (cm^{-1}): 1635, 1613, 1506, 1424, 1181, 1158, 1116, 1099, 1080, 1041, 1030, 941, 897, 837, 825, 792, 767, 703.

Synthesis of Complex [(PyA)Cu(NO_3)$_2$] (PyA-Cu). The ligand (1.17 mmol, 0.434 g) was dissolved in 10 ml of methanol and a water solution (5 ml) of copper(II) nitrate trihydrated (0.95 eq) was added slowly under stirring. The resulting deep blue solution was stirred for 1 hour. Then, the solution was let stand at room temperature until crystals suitable for crystallographic analysis were formed (yield = 52 %). Elemental analysis (%) N 20.61; C 35.35; H 3.93. Calcd for $C_{12}H_{15}CuN_6O_6$: N 20.86; C 35.78; H 3.75. ESI-MS (MeOH/H_2O): *m/z* = 279 $[(L\text{-}H)Cu]^+$ and *m/z* = 139.5 $[LCu]^{2+}$. FTIR-ATR (cm^{-1}): 1606, 1515, 1433, 1172, 1160, 1123, 1106, 1090, 1073, 1028, 1019, 930, 831, 771, 707.

Crystallographic structure determination. Suitable crystals were measured on a Rigaku Oxford Diffraction SuperNova diffractometer at 293K using the CuKα radiation (λ=1.54184 Å). Data collection reduction and multiscan ABSPACK correction were performed with CrysAlisPro (Rigaku Oxford Diffraction). The structures were solved by direct methods with SHELXS and SHELXL[62,63] was used for full matrix least squares refinement. All H-atoms were found experimentally and their coordinates and Uiso parameters were constraint to 1.5Ueq (parent atoms) for the methyls and to 1.2Ueq (parent atom) for the other carbons. Additional crystallographic data can be found in Tables S1 & S2. Crystal structure(s) have been deposited at the Cambridge Crystallographic Data Centre.[64] Deposition Number(s) <url href="https://www.ccdc.cam.ac.uk/services/structures?id=doi:10.1002/##.20220XXX"> 2271674 (for **Pyl-Cu**), 2271673 (for **PyA-Cu**),</url> contain(s) the supplementary crystallographic data for this paper. These data are provided free of charge by the joint Cambridge Crystallographic Data Centre and Fachinformationszentrum Karlsruhe <url href="http://www.ccdc.cam.ac.uk/structures">Access Structures service</url>.

Cyclic voltammetry. Cyclic voltammetry experiments were performed on a Biologic SP-150 potentiostat using a conventional three-electrode system consisting of a glassy carbon (2 mm^2) working electrode, a platinum wire counter electrode and a leakless AgCl/Ag reference electrode (eDAQ). Experiments were conducted in a 5 mL electrochemical cell equipped with an argon-purge system, at room temperature. The complexes were placed at 1 mM concentrations in phosphate buffer at pH 7.5. All the potentials in the text are referred *vs*. SHE.

Electron Paramagnetic Resonance measurements. X-band EPR spectra were measured using an ELEXSYS Bruker instrument equipped with a BVT 3000 digital temperature controller. The complexes were placed in aqueous solutions containing 10% of glycerol at concentrations ranging from 0.2 to 2 mM. Typical acquisition parameters were: temperature: 120K, microwave power 10-20 mW, modulation frequency 100 kHz, modulation gain 3 G. Simulations were performed using the EasySpin toolbox developed for MATLAB.[65]

Activity assay on para-nitrophenyl-beta-(D)-glucopyranoside (*p*-NPG). Activity assays were performed in total volumes of 200 µL placed in 96-well plates. The temperature was set at 30°C. Complexes or $Cu(NO_3)_2.3H_2O$ were placed at concentrations ranging from 0.01 to 0.1 mM concentrations in 10 mM phosphate buffer at pH 7.5. The substrate p-nitrophenyl-β-D-glucopyranoside was used at 10 mM concentration and hydrogen peroxide at concentrations of 10 to 40 mM. Controls were performed using the same conditions, but in the absence of complexes and/or hydrogen peroxide. Absorbances at 400 nm were recorded using a BIOTEK Synergy MX microplate reader. Quantification was performed by measuring the absorbance at 400 nm of solutions of *p*-nitrophenol placed at different concentrations under the same conditions. Assays were reproduced at least 3 times.

Activity assay on cellobiose (G2). Activity assays were performed in total volume of 120 µL. Complexes or $Cu(NO_3)_2.3H_2O$ were placed in 10 mM phosphate buffer pH 7.5. The substrate (G2) was used at 200 µM concentration and hydrogen peroxide at concentrations ranging from 2-50 mM. Controls were performed using the same conditions, but in the absence of complexes and/or hydrogen peroxide. Reaction mixtures were incubated at 30°C and mixed at 1150 rpm in a thermomixer. Ten minutes before injection, 5 nM of catalase were added to stop the reaction. Assays were reproduced at least 3 times. Analysis was performed by high performance anion exchange chromatography (HPAEC) using an ICS 5000+ system (Dionex) and monitored by with pulsed amperometric detection (PAD) and using a CarboPac PA1 2×250 mm analytical column coupled to a CarboPac PA1 2×50 mm guard column. The separation method used in this work was adapted from already reported procedure.[66] Briefly, the products were eluted at a flow rate of 0.25 mL/ min with initial conditions containing 0.1 M NaOH (Eluent A) followed by a stepwise gradient with increasing proportion of 0.1M NaOH and 1M NaOAc (Eluent B). Quantification was performed by using calibration curves. Glucose, Cellobiose and glucoronic acid were purchased from Sigma Life sciences. Gluconic acid and cellobionic acid were obtained after overnight incubation of glucose or cellobiose with 1 µM (0.01eq) Cellobiose Dehydrogenase (CDH), kindly provided by the group of J.-G. Berrin (Biodiversité et Biotechnologie Fongique, INRAE, Marseille). Retention times: glucose (5.8 min), cellobiose (10.9 min), glucoronic acid (21.6 min), gluconic acid (12.9 min) and cellobionic acid (17.0 min).

Activity assay on solid substrates. cellulose, chitin and bagasse. 20 mg of cellulose/chitin or 40 mg of bagasse were placed in 1.75 mL of 10 mM phosphate buffer at pH 7.5 in the presence of complexes and hydrogen peroxide. Reaction mixtures were incubated at 30°C under stirring at 1150 rpm. At the end of reaction, the mixtures were centrifugated, the supernatants were removed and the remaining solids were dried at 50°C for at least 24h until no more weight evolution was observed. The final weights of the solid substrate were compared to the initial ones to evaluate the weight loss in %. Controls were performed using $Cu(NO_3)_2.3H_2O$ instead of the complexes or using only hydrogen peroxide alone. Assays were reproduced at least 3 times. The supernatants were filtrated on celite and treated with catalase to remove excess hydrogen peroxide. They were analyzed by high performance anion exchange chromatography (HPAEC) as described above (cellobiose assay). Further analysis by HPLC-ELSD was carried out on an Agilent 1260 Infinity II chromatograph at an evaporator temperature of 80 °C, nebulizer temperature 40 °C, and column temperature 60 °C; a Hi-Plex H column (30 × 7.7 mm) was used with water as eluant at 0.6 mL min^{-1}.

Hydroxyl radical detection assay. 5 mM stock solutions of Coumarin-3-Carboxylic Acid (CCA) were prepared in 50 mM phosphate buffer at pH 8.5. Assays were performed in final volumes of 200 µL in 50 mM phosphate buffer at pH 7.4 using 500 µM of CCA and 10 µM of complexes. Fluorescence measurements were performed on a FLUOstar Optima 96-well plate reader system (BMG Labtech) at 25°C. The fluorescence was monitored every 30 seconds at 452 nm upon excitation at 395 nm. An automatic injector was used to add hydrogen peroxide solutions into the wells during experiments. The addition was performed in one or two injections of volumes ranging from 2-8 µL to reach final concentrations of 0.1 to 5 mM. Each condition was reproduced 3 times.

Supporting Information

The authors have cited additional reference within the Supporting Information.[67]

Acknowledgements

The authors are grateful to ECOS-NORD and CONAHCYT for the bilateral funded project (M17P01, 291247). The authors acknowledge Region-Sud PACA for the Ph.D fellowship of R.L. and CONAHCYT for funding and the PhD fellowship of R.D. (A1-S-8682). R.L. is grateful for the travel support provided by FrenchBic (http://frenchbic.cnrs.fr). Finally, the authors thank S. Grisel and J.-G. Berrin from INRAE Marseille for advices and for providing CDH enzyme and Carmen Márquez for her help in HPLC-ELSD.

Keywords: copper • bioinspired catalysis • LPMO • polysaccharide • oxidation

[1] M. S. Singhvi, D. V. Gokhale, *Appl Microbiol Biotechnol* **2019**, *103*, 9305–9320.
[2] D. W. Wakerley, M. F. Kuehnel, K. L. Orchard, K. H. Ly, T. E. Rosser, E. Reisner, *Nat Energy* **2017**, *2*, 17021.
[3] K. K. Meier, S. M. Jones, T. Kaper, H. Hansson, M. J. Koetsier, S. Karkehabadi, E. I. Solomon, M. Sandgren, B. Kelemen, *Chem. Rev.* **2018**, *118*, 2593–2635.
[4] G. Vaaje-Kolstad, B. Westereng, S. J. Horn, Z. Liu, H. Zhai, M. Sørlie, V. G. H. Eijsink, *Science* **2010**, *330*, 219–222.
[5] Z. Forsberg, M. Sørlie, D. Petrović, G. Courtade, F. L. Aachmann, G. Vaaje-Kolstad, B. Bissaro, Å. K. Røhr, V. G. Eijsink, *Curr. Opin. Struct. Biol.* **2019**, *59*, 54–64.
[6] G. R. Hemsworth, E. M. Johnston, G. J. Davies, P. H. Walton, *Trends Biotechnol.* **2015**, *33*, 747–761.
[7] T. Tandrup, K. E. H. Frandsen, K. S. Johansen, J.-G. Berrin, L. L. Leggio, *Biochem. Soc. Trans.* **2018**, *46*, 1431–1447.
[8] B. Bissaro, Å. K. Røhr, G. Müller, P. Chylenski, M. Skaugen, Z. Forsberg, S. J. Horn, G. Vaaje-Kolstad, V. G. H. Eijsink, *Nat. Chem. Biol.* **2017**, *13*, 1123–1128.
[9] W. T. Beeson, C. M. Phillips, J. H. D. Cate, M. A. Marletta, *J. Am. Chem. Soc.* **2012**, *134*, 890–892.
[10] A. Villares, C. Moreau, C. Bennati-Granier, S. Garajova, L. Foucat, X. Falourd, B. Saake, J.-G. Berrin, B. Cathala, *Sci Rep* **2016**, 1–9.
[11] M. Chemin, K. Kansou, K. Cahier, M. Grellier, S. Grisel, B. Novales, C. Moreau, A. Villares, J.-G. Berrin, B. Cathala, *Biomacromol.* **2023**, DOI 10.1021/acs.biomac.3c00303.
[12] E. Drula, M.-L. Garron, S. Dogan, V. Lombard, B. Henrissat, N. Terrapon, *Nucleic Acids Res.* **2021**, *50*, D571–D577.
[13] P. H. Walton, G. J. Davies, D. E. Diaz, J. P. Franco-Cairo, *FEBS Lett* **2023**, *597*, 485–494.
[14] L. Ciano, G. J. Davies, W. B. Tolman, P. H. Walton, *Nat. Catal.* **2018**, *1*, 571–577.
[15] A. Munzone, B. E. Kerdi, M. Fanuel, H. Rogniaux, D. Ropartz, M. Réglier, A. Royant, A. J. Simaan, C. Decroos, *FEBS J.* **2020**, *287*, 3298–3314.
[16] B. Bissaro, V. G. H. Eijsink, *Essays Biochem* 2023, *67*, 575–584.
[17] B. Wang, Z. Wang, G. J. Davies, P. H. Walton, C. Rovira, *ACS Catal.* **2020**, *10*, 12760–12769.
[18] T. M. Hedison, E. Breslmayr, M. Shanmugam, K. Karnpakdee, D. J. Heyes, A. P. Green, R. Ludwig, N. S. Scrutton, D. Kracher, *FEBS J.* **2021**, *288*, 4115–4128.
[19] J. A. Hangasky, A. T. Iavarone, M. A. Marletta, *Proc. Natl. Acad. Sci.* **2018**, *115*, 4915–4920.
[20] B. Wang, E. M. Johnston, P. Li, S. Shaik, G. J. Davies, P. H. Walton, C. Rovira, *ACS Catal.* **2018**, *8*, 1346–1351.
[21] B. Wang, X. Zhang, W. Fang, C. Rovira, S. Shaik, *Acc. Chem. Res.* **2022**, *55*, 2280–2290.
[22] S. M. Adam, G. B. Wijeratne, P. J. Rogler, D. E. Diaz, D. A. Quist, J. J. Liu, K. D. Karlin, *Chem. Rev.* **2018**, *118*, 10840–11022.
[23] C. E. Elwell, N. L. Gagnon, B. D. Neisen, D. Dhar, A. D. Spaeth, G. M. Yee, W. B. Tolman, *Chem. Rev.* **2017**, *117*, 2059–2107.
[24] S. Itoh, *Acc. Chem. Res.* **2015**, *48*, 2066–2074.
[25] A. L. Concia, A. Munzone, M.-C. Kafentzi, A. Kochem, M. Reglier, C. Decroos, A. J. Simaan, *Modeling the Mononuclear Copper Monooxygenase Active Site*, in Bioinspired Chemistry, World Scientific book, **2019**.
[26] W. Keown, J. B. Gary, T. D. P. Stack, *J. Biol. Inorg. Chem.* **2016**, *22*, 289–305.
[27] D. A. Quist, D. E. Diaz, J. J. Liu, K. D. Karlin, *J. Biol. Inorg. Chem.* **2016**, *22*, 253–288.
[28] A. L. Concia, M. R. Beccia, M. Orio, F. T. Ferre, M. Scarpellini, F. Biaso, B. Guigliarelli, M. Réglier, A. J. Simaan, *Inorg. Chem.* **2017**, *56*, 1023–1026.
[29] I. Castillo, A. C. Neira, E. Nordlander, E. Zeglio, *Inorg. Chim. Acta* **2014**, *422*, 152–157.
[30] A. C. Neira, P. R. Martínez-Alanis, G. Aullón, M. Flores-Alamo, P. Zerón, A. Company, J. Chen, J. B. Kasper, W. R. Browne, E. Nordlander, I. Castillo, *ACS Omega* **2019**, *4*, 10729–10740.
[31] S. Muthuramalingam, D. Maheshwaran, M. Velusamy, R. Mayilmurugan, *J. Catal.* **2019**, *372*, 352–361.
[32] A. Fukatsu, Y. Morimoto, H. Sugimoto, S. Itoh, *Chem. Commun*. **2020**, *56*, 5123–5126.
[33] Z. Yu, Z. Thompson, S. L. Behnke, K. D. Fenk, D. Huang, H. S. Shafaat, J. A. Cowan, *Inorg Chem* **2020**, *59*, 11218–11222.
[34] I. Castillo, A. P. Torres-Flores, D. F. Abad-Aguilar, A. Berlanga-Vázquez, M. Orio, D. Martínez-Otero, *Chemcatchem* **2021**, *13*, 4700–4704.
[35] K. Chen, M. Zangiabadi, Y. Zhao, *Org Lett* **2022**, *24*, 3426–3430.
[36] C. J. Bouchey, D. Y. Shopov, A. D. Gruen, W. B. Tolman, *ACS Omega* **2022**, *7*, 35217–35232.
[37] B. Servaramuthu, T. Nagendraraj, J. Annaraj, *Orient. J. Chem.* **2023**, *39*, 497–504.
[38] J. Saikia, V. T. Bhat, L. R. Potnuru, A. S. Redkar, V. Agarwal, V. Ramakrishnan, *ACS Omega* **2022**, *7*, 19131–19140.
[39] A. A. Hassoon, A. Szorcsik, L. Fülöp, Z. I. Papp, N. V. May, T. Gajda, *Dalton Trans.* **2022**, *51*, 17241–17254.
[40] R. Peifer, L. Müller, S. Hoof, F. Beckmann, B. Cula, C. Limberg, *Zeits. Anorg. Allg. Chem.* **2021**, *647*, 1789–1796.
[41] J. Peisach, W. E. Blumberg, *Arch. Biochem Biophys.* **1974**, *165*, 691–708.
[42] U. Sakaguchi, A. W. Addison, *J. Chem. Soc., Dalton Trans.* **1979**, 600–9.
[43] F. L. Aachmann, M. Sørlie, G. Skjåk-Bræk, V. G. H. Eijsink, G. Vaaje-Kolstad, *Proc. Natl. Acad. Sci.* **2012**, *109*, 18779–18784.
[44] A. S. Borisova, T. Isaksen, M. Dimarogona, A. A. Kognole, G. Mathiesen, A. Várnai, Å. K. Røhr, C. M. Payne, M. Sørlie, M. Sandgren, V. G. H. Eijsink, *J. Biol. Chem.* **2015**, *290*, 22955–22969.
[45] S. Garajova, Y. Mathieu, M. R. Beccia, C. Bennati-Granier, F. Biaso, M. Fanuel, D. Ropartz, B. Guigliarelli, E. Record, H. Rogniaux, B. Henrissat, J.-G. Berrin, *Sci. Rep.* **2016**, *6*, 28276.
[46] D. Zouraris, M. Dimarogona, A. Karnaouri, E. Topakas, A. Karantonis, *Bioelectrochem.* **2018**, *124*, 149–155.
[47] L. Rieder, D. Petrović, P. Väljamäe, V. G. H. Eijsink, M. Sørlie, *ACS Catal* **2021**, *11*, 11685–11695.
[48] C. M. Cordas, G. N. Valério, A. Stepnov, E. Kommedal, Å. R. Kjendseth, Z. Forsberg, V. G. H. Eijsink, J. J. G. Moura, *J Inorg Biochem* **2023**, *238*, 112056.
[49] R. Palomo-Briones, I. López-Gutiérrez, F. Islas-Lugo, K. L. Galindo-Hernández, D. Munguía-Aguilar, J. A. Rincón-Pérez, M. Á. Cortés-Carmona, F. Alatriste-Mondragón, E. Razo-Flores, *Clean Technol. Environ. Polic.* **2018**, *20*, 1423–1441.
[50] B. Wang, X. Zhang, W. Fang, C. Rovira, S. Shaik, *Acc. Chem. Res.* 2022, *55*, 2280–2290.
[51] D. T. Sawyer, A. Sobkowiak, T. Matsushita, *Acc. Chem. Res.* **1996**, *29*, 409–416.
[52] A. N. Pham, G. Xing, C. J. Miller, T. D. Waite, *J. Catal.* **2013**, *301*, 54–64.
[53] M. Hayyan, M. A. Hashim, I. M. AlNashef, *Chem. Rev.* **2016**, *116*, 3029–3085.
[54] C. Cheignon, F. Collin, P. Faller, C. Hureau, *Dalton Trans.* **2016**, *45*, 12627–12631.
[55] C. Cheignon, P. Faller, D. Testemale, C. Hureau, F. Collin, *Metallomics* **2016**, *8*, 1081–1089.
[56] S. Zhang, R. Trammell, A. Cordova, M. A. Siegler, I. Garcia-Bosch, *J Inorg Biochem* **2021**, *223*, 111557.

10.1002/cctc.202300933

[57] W. Ghattas, M. Giorgi, Y. Mekmouche, T. Tanaka, A. Rockenbauer, M. Réglier, Y. Hitomi, A. J. Simaan, *Inorg. Chem.* **2008**, *47*, 4627–4638.
[58] B. Kim, M. T. Brueggemeyer, W. J. Transue, Y. Park, J. Cho, M. A. Siegler, E. I. Solomon, K. D. Karlin, *J. Am. Chem. Soc.* **2023**, *145*, 11735–11744.
[59] F. Filandr, D. Kavan, D. Kracher, C. V. F. P. Laurent, R. Ludwig, P. Man, P. Halada, *Biomol* **2020**, *10*, 242.
[60] A. Paradisi, E. M. Johnston, M. Tovborg, C. R. Nicoll, L. Ciano, A. Dowle, J. McMaster, Y. Hancock, G. J. Davies, P. H. Walton, *J Am Chem Soc* **2019**, *141*, 18585–18599.
[61] D. M. Petrović, B. Bissaro, P. Chylenski, M. Skaugen, M. Sørlie, M. S. Jensen, F. L. Aachmann, G. Courtade, A. Várnai, V. G. H. Eijsink, *Prot. Sci.* **2018**, *27*, 1636–1650.
[62] G. M. Sheldrick, *Acta Crystallogr. Sect. A: Found. Crystallogr.* **2008**, *64*, 112–122.
[63] G. M. Sheldrick, *Acta Crystallogr C Struct Chem* **2015**, *71*, 3–8.
[64] Deposition numbers 2271673 (**PyA-Cu**) and 2271674 (**PyI-Cu**) contain the supplementary crystallographic data for this paper. These data are provided free of charge by the Cambridge Crystallographic Data Centre.
[65] S. Stoll, A. Schweiger, *J. Magn. Reson.* **2006**, *178*, 42–55.
[66] B. Westereng, J. W. Agger, S. J. Horn, G. Vaaje-Kolstad, F. L. Aachmann, Y. H. Stenstrøm, V. G. H. Eijsink, *J. Chromatogr. A* **2013**, *1271*, 144–152.
[67] A. A. Stepnov, I. A. Christensen, Z. Forsberg, F. L. Aachmann, G. Courtade, V. G. H. Eijsink, *FEBS Lett*. **2022**, *596*, 53–70.

10.1002/cctc.202300933

WILEY VCH

RESEARCH ARTICLE

Entry for the Table of Contents

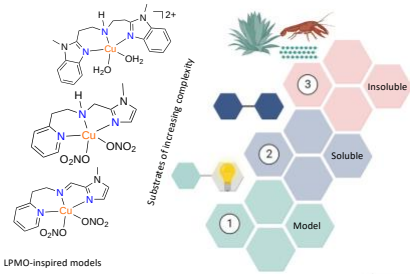

The catalytic activity of several LPMO-bioinspired copper complexes was assayed on different substrates of increasing complexity (soluble to extended insoluble polysaccharides). The different assays are compared and proof-of-concept that bioinspired complexes can oxidatively promote polysaccharide depolymerization was obtained. Mechanistic pathways and catalysts stability are discussed.

Twitters:
@jsimaan1
@ism2_fr
@IvanCas68860420
@rbk_lbly
@BioInorgani
@axadrian

[1] M. S. Singhvi, D. V. Gokhale, *Appl Microbiol Biotechnol* **2019**, *103*, 9305–9320.

[2] D. W. Wakerley, M. F. Kuehnel, K. L. Orchard, K. H. Ly, T. E. Rosser, E. Reisner, *Nat Energy* **2017**, *2*, 17021.

[3] K. K. Meier, S. M. Jones, T. Kaper, H. Hansson, M. J. Koetsier, S. Karkehabadi, E. I. Solomon, M. Sandgren, B. Kelemen, *Chem. Rev.* **2018**, *118*, 2593–2635.

[4] G. Vaaje-Kolstad, B. Westereng, S. J. Horn, Z. Liu, H. Zhai, M. Sørlie, V. G. H. Eijsink, *Science* **2010**, *330*, 219–222.

[5] Z. Forsberg, M. Sørlie, D. Petrović, G. Courtade, F. L. Aachmann, G. Vaaje-Kolstad, B. Bissaro, Å. K. Røhr, V. G. Eijsink, *Curr. Opin. Struct. Biol.* **2019**, *59*, 54–64.

[6] G. R. Hemsworth, E. M. Johnston, G. J. Davies, P. H. Walton, *Trends Biotechnol.* **2015**, *33*, 747–761.

[7] T. Tandrup, K. E. H. Frandsen, K. S. Johansen, J.-G. Berrin, L. L. Leggio, *Biochem. Soc. Trans.* **2018**, *46*, 1431–1447.

[8] B. Bissaro, Å. K. Røhr, G. Müller, P. Chylenski, M. Skaugen, Z. Forsberg, S. J. Horn, G. Vaaje-Kolstad, V. G. H. Eijsink, *Nat. Chem. Biol.* **2017**, *13*, 1123–1128.

[9] W. T. Beeson, C. M. Phillips, J. H. D. Cate, M. A. Marletta, *J. Am. Chem. Soc.* **2012**, *134*, 890–892.

[10] A. Villares, C. Moreau, C. Bennati-Granier, S. Garajova, L. Foucat, X. Falourd, B. Saake, J.-G. Berrin, B. Cathala, *Sci Rep* **2016**, 1–9.

[11] M. Chemin, K. Kansou, K. Cahier, M. Grellier, S. Grisel, B. Novales, C. Moreau, A. Villares, J.-G. Berrin, B. Cathala, *Biomacromolecules* **2023**, DOI 10.1021/acs.biomac.3c00303.

[12] E. Drula, M.-L. Garron, S. Dogan, V. Lombard, B. Henrissat, N. Terrapon, *Nucleic Acids Res.* **2021**, *50*, D571–D577.

[13] P. H. Walton, G. J. Davies, D. E. Diaz, J. P. Franco-Cairo, *Febs Lett* **2023**, *597*, 485–494.

[14] L. Ciano, G. J. Davies, W. B. Tolman, P. H. Walton, *Nat. Catal.* **2018**, *1*, 571–577.

[15] A. Munzone, B. E. Kerdi, M. Fanuel, H. Rogniaux, D. Ropartz, M. Réglier, A. Royant, A. J. Simaan, C. Decroos, *FEBS J.* **2020**, *287*, 3298–3314.

[16] B. Bissaro, V. G. H. Eijsink, *Essays Biochem* **2023**, *67*, 575–584.

[17] B. Wang, Z. Wang, G. J. Davies, P. H. Walton, C. Rovira, *ACS Catal.* **2020**, *10*, 12760–12769.

[18] T. M. Hedison, E. Breslmayr, M. Shanmugam, K. Karnpakdee, D. J. Heyes, A. P. Green, R. Ludwig, N. S. Scrutton, D. Kracher, *FEBS J.* **2021**, *288*, 4115–4128.

[19] J. A. Hangasky, A. T. Iavarone, M. A. Marletta, *Proc. Natl. Acad. Sci.* **2018**, *115*, 4915–4920.

[20] B. Wang, E. M. Johnston, P. Li, S. Shaik, G. J. Davies, P. H. Walton, C. Rovira, *Acs Catal* **2018**, *8*, 1346–1351.

[21] B. Wang, X. Zhang, W. Fang, C. Rovira, S. Shaik, *Acc. Chem. Res.* **2022**, *55*, 2280–2290.

[22] S. M. Adam, G. B. Wijeratne, P. J. Rogler, D. E. Diaz, D. A. Quist, J. J. Liu, K. D. Karlin, *Chem. Rev.* **2018**, *118*, 10840–11022.

[23] C. E. Elwell, N. L. Gagnon, B. D. Neisen, D. Dhar, A. D. Spaeth, G. M. Yee, W. B. Tolman, *Chem. Rev.* **2017**, *117*, 2059–2107.

[24] S. Itoh, *Acc. Chem. Res.* **2015**, *48*, 2066–2074.

[25] A. L. Concia, A. Munzone, M.-C. Kafentzi, A. Kochem, M. Reglier, C. Decroos, A. J. Simaan, *Modeling the Mononuclear Copper Monooxygenase Active Site*, World Scientific, **2019**.

[26] W. Keown, J. B. Gary, T. D. P. Stack, *J Biol Inorg Chem* **2016**, *22*, 289–305.

[27] D. A. Quist, D. E. Diaz, J. J. Liu, K. D. Karlin, *J Biol Inorg Chem* **2016**, *22*, 253–288.

[28] A. L. Concia, M. R. Beccia, M. Orio, F. T. Ferre, M. Scarpellini, F. Biaso, B. Guigliarelli, M. Réglier, A. J. Simaan, *Inorg. Chem.* **2017**, *56*, 1023–1026.

[29] I. Castillo, A. C. Neira, E. Nordlander, E. Zeglio, *Inorg. Chim. Acta* **2014**, *422*, 152–157.

[30] A. C. Neira, P. R. Martínez-Alanis, G. Aullón, M. Flores-Alamo, P. Zerón, A. Company, J. Chen, J. B. Kasper, W. R. Browne, E. Nordlander, I. Castillo, *ACS Omega* **2019**, *4*, 10729–10740.

[31] S. Muthuramalingam, D. Maheshwaran, M. Velusamy, R. Mayilmurugan, *J. Catal.* **2019**, *372*, 352–361.

[32] A. Fukatsu, Y. Morimoto, H. Sugimoto, S. Itoh, *Chem. Commun.* **2020**, *56*, 5123–5126.

[33] Z. Yu, Z. Thompson, S. L. Behnke, K. D. Fenk, D. Huang, H. S. Shafaat, J. A. Cowan, *Inorg Chem* **2020**, *59*, 11218–11222.

[34] I. Castillo, A. P. Torres-Flores, D. F. Abad-Aguilar, A. Berlanga-Vázquez, M. Orio, D. Martínez-Otero, *Chemcatchem* **2021**, *13*, 4700–4704.

[35] K. Chen, M. Zangiabadi, Y. Zhao, *Org Lett* **2022**, *24*, 3426–3430.

[36] C. J. Bouchey, D. Y. Shopov, A. D. Gruen, W. B. Tolman, *Acs Omega* **2022**, *7*, 35217–35232.

[37] B. Servaramuthu, T. Nagendraraj, J. Annaraj, *Orient. J. Chem.* **2023**, *39*, 497–504.

[38] J. Saikia, V. T. Bhat, L. R. Potnuru, A. S. Redkar, V. Agarwal, V. Ramakrishnan, *Acs Omega* **2022**, *7*, 19131–19140.

[39] A. A. Hassoon, A. Szorcsik, L. Fülöp, Z. I. Papp, N. V. May, T. Gajda, *Dalton Trans.* **2022**, *51*, 17241–17254.

[40] R. Peifer, L. Müller, S. Hoof, F. Beckmann, B. Cula, C. Limberg, *Zeitschrift für Anorg. und allgemeine Chemie* **2021**, *647*, 1789–1796.

[41] J. Peisach, W. E. Blumberg, *Arch. Biochem Biophys.* **1974**, *165*, 691–708.

[42] U. Sakaguchi, A. W. Addison, *J. Chem. Soc., Dalton Trans.* **1979**, 600–9.

[43] F. L. Aachmann, M. Sørlie, G. Skjåk-Bræk, V. G. H. Eijsink, G. Vaaje-Kolstad, *Proc. Natl. Acad. Sci.* **2012**, *109*, 18779–18784.

[44] A. S. Borisova, T. Isaksen, M. Dimarogona, A. A. Kognole, G. Mathiesen, A. Várnai, Å. K. Røhr, C. M. Payne, M. Sørlie, M. Sandgren, V. G. H. Eijsink, *J. Biol. Chem.* **2015**, *290*, 22955–22969.

[45] S. Garajova, Y. Mathieu, M. R. Beccia, C. Bennati-Granier, F. Biaso, M. Fanuel, D. Ropartz, B. Guigliarelli, E. Record, H. Rogniaux, B. Henrissat, J.-G. Berrin, *Sci Rep* **2016**, *6*, 28276.

[46] D. Zouraris, M. Dimarogona, A. Karnaouri, E. Topakas, A. Karantonis, *Bioelectrochemistry* **2018**, *124*, 149–155.

[47] L. Rieder, D. Petrović, P. Väljamäe, V. G. H. Eijsink, M. Sørlie, *Acs Catal* **2021**, *11*, 11685–11695.

[48] C. M. Cordas, G. N. Valério, A. Stepnov, E. Kommedal, Å. R. Kjendseth, Z. Forsberg, V. G. H. Eijsink, J. J. G. Moura, *J Inorg Biochem* **2023**, *238*, 112056.

[49] R. Palomo-Briones, I. López-Gutiérrez, F. Islas-Lugo, K. L. Galindo-Hernández, D. Munguía-Aguilar, J. A. Rincón-Pérez, M. Á. Cortés-Carmona, F. Alatriste-Mondragón, E. Razo-Flores, *Clean Technol. Environ. Polic.* **2018**, *20*, 1423–1441.

[50] B. Wang, X. Zhang, W. Fang, C. Rovira, S. Shaik, *Accounts Chem Res* **2022**, *55*, 2280–2290.

[51] D. T. Sawyer, A. Sobkowiak, T. Matsushita, *Acc. Chem. Res.* **1996**, *29*, 409–416.

[52] A. N. Pham, G. Xing, C. J. Miller, T. D. Waite, *J. Catal.* **2013**, *301*, 54–64.

[53] M. Hayyan, M. A. Hashim, I. M. AlNashef, *Chem. Rev.* **2016**, *116*, 3029–3085.

[54] C. Cheignon, F. Collin, P. Faller, C. Hureau, *Dalton Trans.* **2016**, *45*, 12627–12631.

[55] C. Cheignon, P. Faller, D. Testemale, C. Hureau, F. Collin, *Metallomics* **2016**, *8*, 1081–1089.

[56] S. Zhang, R. Trammell, A. Cordova, M. A. Siegler, I. Garcia-Bosch, *J Inorg Biochem* **2021**, *223*, 111557.

[57] W. Ghattas, M. Giorgi, Y. Mekmouche, T. Tanaka, A. Rockenbauer, M. Réglier, Y. Hitomi, A. J. Simaan, *Inorg. Chem.* **2008**, *47*, 4627–4638.

[58] B. Kim, M. T. Brueggemeyer, W. J. Transue, Y. Park, J. Cho, M. A. Siegler, E. I. Solomon, K. D. Karlin, *J. Am. Chem. Soc.* **2023**, *145*, 11735–11744.

[59] F. Filandr, D. Kavan, D. Kracher, C. V. F. P. Laurent, R. Ludwig, P. Man, P. Halada, *Biomol* **2020**, *10*, 242.

[60] A. Paradisi, E. M. Johnston, M. Tovborg, C. R. Nicoll, L. Ciano, A. Dowle, J. McMaster, Y. Hancock, G. J. Davies, P. H. Walton, *J Am Chem Soc* **2019**, *141*, 18585–18599.

[61] D. M. Petrović, B. Bissaro, P. Chylenski, M. Skaugen, M. Sørlie, M. S. Jensen, F. L. Aachmann, G. Courtade, A. Várnai, V. G. H. Eijsink, *Protein Sci.* **2018**, *27*, 1636–1650.

[62] G. M. Sheldrick, *Acta Crystallogr. Sect. A: Found. Crystallogr.* **2008**, *64*, 112–122.

[63] G. M. Sheldrick, *Acta Crystallogr C Struct Chem* **2015**, *71*, 3–8.

[64] L. Brisson, N. Bakkali-Taheri, M. Giorgi, A. Fadel, J. Kaizer, M. Réglier, T. Tron, E. H. Ajandouz, A. J. Simaan, *J Biol Inorg Chem* **2012**, *17*, 939–949.

[65] S. Stoll, A. Schweiger, *J. Magn. Reson.* **2006**, *178*, 42–55.

[66] B. Westereng, J. W. Agger, S. J. Horn, G. Vaaje-Kolstad, F. L. Aachmann, Y. H. Stenstrøm, V. G. H. Eijsink, *J. Chromatogr. A* **2013**, *1271*, 144–152.

[67] A. A. Stepnov, I. A. Christensen, Z. Forsberg, F. L. Aachmann, G. Courtade, V. G. H. Eijsink, *FEBS Lett.* **2022**, *596*, 53–70.